PROCEEDINGS OF SPIE

SPIEDigitalLibrary.org/conference-proceedings-of-spie

Tolerance analysis of a self-coherent camera for wavefront sensing and dark hole maintenance

Kevin Derby, Sebastiaan Haffert, Jaren Ashcraft, Kian Milani, Heejoo Choi, et al.

Kevin Z. Derby, Sebastiaan Haffert, Jaren Ashcraft, Kian Milani, Heejoo Choi, Young-Sik Kim, Laird Close, Christopher Mendillo, Supriya Chakrabarti, Gregory Allan, Leonid Pogorelyuk, Kerri Cahoy, Mamadou N'Diaye, Daewook Kim, Jared Males, Ewan Douglas, "Tolerance analysis of a self-coherent camera for wavefront sensing and dark hole maintenance," Proc. SPIE 12180, Space Telescopes and Instrumentation 2022: Optical, Infrared, and Millimeter Wave, 1218069 (27 August 2022); doi: 10.1117/12.2629578

SPIE.

Event: SPIE Astronomical Telescopes + Instrumentation, 2022, Montréal, Québec, Canada

Tolerance analysis of a self-coherent camera for wavefront sensing and dark hole maintenance

Kevin Z. Derby[a], Sebastiaan Haffert[a], Jaren Ashcraft[a], Kian Milani[a], Heejoo Choi[a,b], Youngsik Kim[a], Laird Close[b], Christopher Mendillo[d], Supriya Chakrabarti[d], Greg Allan[e], Leonid Pogorelyuk[e], Kerri Cahoy[e], Mamadou N'Diaye[f], Daewook Kim[a,b,c], Jared Males[c], and Ewan Douglas[c]

[a]Wyant College of Optical Sciences, University of Arizona, Tucson, AZ, USA
[b]Large Binocular Telescope Observatory, University of Arizona, Tucson, AZ, USA
[c]Department of Astronomy and Steward Observatory, University of Arizona, Tucson, AZ, USA
[d]Lowell Center for Space Science and Technology, University of Massachusetts Lowell, Lowell, MA, USA
[e]Department of Aeronautics and Astronautics, Massachusetts Institute of Technology, Cambridge, MA, USA
[f]Observatoire de la Côte d'Azur, 96 Bd de l'Observatoire, 06300 Nice, France

ABSTRACT

Exceptional wavefront correction is required for coronagraphs on future space observatories to reach 10^{-10} contrasts for direct imaging of rocky exoplanets around Sun-like stars. This picometer level wavefront correction must be stable over long periods of time and should be limited only by photon noise and wavefront sensing architecture. Thus, wavefront errors that arise from optical surface errors, thermal gradients, pointing induced beamwalk, and polarization aberration must be tightly controlled.

A self-coherent camera (SCC) allows for image plane correction of mid-spatial frequency errors and a continuous means of dark-hole maintenance. By introducing a reference pinhole at the Lyot stop of a coronagraph, coherent starlight can be interfered with image plane speckles while leaving incoherent planet light untouched. A coronagraph model was created using High Contrast Imaging in Python (HCIPy) to simulate the SCC. Using these tools, realistic input disturbances can be introduced to analyze wavefront sensor performance. Using our model, we first demonstrate the necessity of a complimentary low-order wavefront sensor (LOWFS) to be paired with the SCC. Next, we discuss considerations when creating the modified Lyot stop of an SCC. Finally, a tolerance analysis of the SCC in the presence of optical surface errors, beamwalk due to pointing errors, photon noise, and detector read noise is presented.

Keywords: Self-coherent camera, wavefront sensing, wavefront control, physical optics modeling, high-contrast imaging, coronagraphy

1. INTRODUCTION

Terrestrial exoplanets are typically 10^{10} times fainter than, and separated by fractions of an arcsecond from their host star.[1,2] To achieve such high contrast, coronagraphs are used to attenuate starlight to allow for exoplanet detection at small separations.[3,4] However, these instruments are incredibly sensitive to wavefront errors which leak starlight in the form of image plane speckles. These speckles can obfuscate high-contrast objects of interest, requiring the ability to sense and control wavefront errors to picometer-level stability in order to suppress these leaks.[5]

Adaptive optics (AO) provide a solution to this challenge. In coronagraphs, an AO system is typically comprised of one (or several) wavefront sensors and a deformable mirror (DM) for wavefront correction. These

Further author information: (Send correspondence to E.S.D)
E.S.D.: E-mail: douglase@arizona.edu

Space Telescopes and Instrumentation 2022: Optical, Infrared, and Millimeter Wave, edited by Laura E. Coyle, Shuji Matsuura, Marshall D. Perrin, Proc. of SPIE Vol. 12180, 1218069 · © 2022 SPIE · 0277-786X · doi: 10.1117/12.2629578

can operate in closed-loop control to suppress both static and dynamic speckles at the image plane. Static speckle can arise from imperfections in the system, such as optical surface errors[6] and polarization aberration.[7] For telescopes on the ground, atmospheric turbulence is the dominant source of dynamic speckles.[1,8] However for space-based telescopes, beamwalk due to pointing errors,[9] and changing temperature gradients[10] predominate to cause quasi-static speckles.

Several methods of compensation for these errors using closed-loop wavefront control have been introduced, including pairwise probing (PW) in tandem with stroke minimization or electric field conjugation (EFC) algorithms.[11–13] These sense the wavefront using pairs of images taken after introducing DM probes, then calculating the DM shape required to minimize the amount of residual starlight within a specified region of the image known as the "dark hole". It is important to note that (PW) probing requires at least four images corresponding to two probes.[11] Ideally, using more probes would leads to a more accurate estimation of the wavefront. However, the number of probes should be minimized to prevent contamination of the science image during data acquisition. In addition, on dim targets especially, the limited number of photons leads to long exposure times being necessary for a single image, leading to a slow wavefront correction loop which is more susceptible to quasi-static speckles.

1.1 The Self-Coherent Camera

The a self-coherent camera (SCC) is an image plane wavefront sensing method capable of correcting mid-spatial frequency speckles and continuously maintaining a dark hole.[14–18] It operates by creating a reference channel using a pinhole at the Lyot stop, allowing a small amount of starlight through to the science image. This starlight will interfere with quasi-static speckles due to coherence, while leaving incoherent planet and exozodiacal light untouched. This difference in coherence also opens possibilities for post-data acquisition image processing using coherent differential imaging (CDI).[19–21]

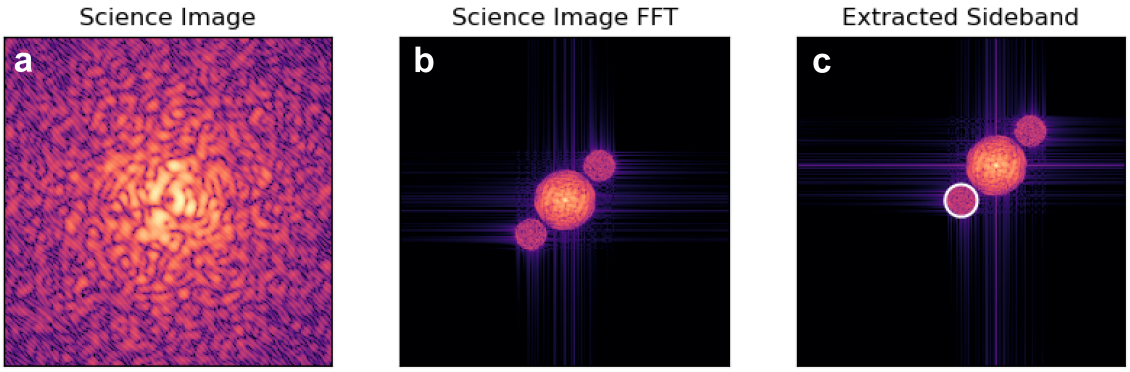

Figure 1. Wavefront sensing using an SCC. The pinhole at the Lyot plane allows starlight to interfere with spekles at the (a) science image. The (b) FT of the science image shows three peaks. (c) One of the lateral peaks can be centered and isolated. The inverse FT of this extracted peak results in an estimation of stellar speckles.

The Fourier Transform (FT) of an SCC image results in three peaks which will not overlap if the separation between the pinhole and Lyot stop is large enough. In this case, one of the lateral peaks can be centered and isolated. The inverse FT of this extracted peak results in an estimation of stellar speckles using only a single science image. This ability to sense quasi-static image plane speckles using a single image by simply introducing a pinhole at the Lyot stop makes the SCC an attractive and elegant solution for faster dark-hole maintenance on future space-based coronagraphs.

In the following sections, we model a 6 meter unobstructed telescope and coronagraph instrument. Using this model, we first demonstrate the necessity of a complimentary low-order wavefront sensor (LOWFS) to be paired with the SCC. Next, we discuss considerations when creating the modified Lyot stop of an SCC. Finally, a tolerance analysis of the SCC in the presence of optical surface errors, beamwalk due to pointing errors, photon noise, and detector read noise is presented. This work is motivated by ongoing technology development necessary for achieving 10^{-10} contrast on a 6 meter class observatory as referenced in the 2021 Decadal survey.[22]

2. PHYSICAL OPTICS PROPAGATION AND MODELING

High Contrast Imaging in Python (HCIPy)[23] is an open-source Python library primarily developed by astronomers at Leiden University. It is are open to contributions from scientists and software developers around the world, and is used to simulate physical optics propagation. It can propagate wavefronts through optical systems using either Fraunhofer or Fresnel approximations of scalar electromagnetic theory.

2.1 Telescope and Instrument Model

An unobscured, circular monolithic aperture measuring 6 meters in diameter (D_{pupil}) was modeled using HCIPy. A 2% bandwidth wavefront ($\lambda_0 = 550$ nm) was first sent a binary aperture mask. Next, a phase screen injected wavefront error into the system which was then corrected by a 32 by 32 actuator DM. The phase screen could be translated laterally to emulate beamwalk caused by telescope pointing errors. The corrected wavefront was then propagated to a focal plane mask and Lyot stop for starlight rejection. For the focal plane mask, a charge-6 vector vortex phase plate was used. The Lyot stop consisted of a central aperture with diameter D_{lyot} and an off-axis pinhole at separation l with a diameter of D_{pin}. A general system layout is shown in Figure 2.

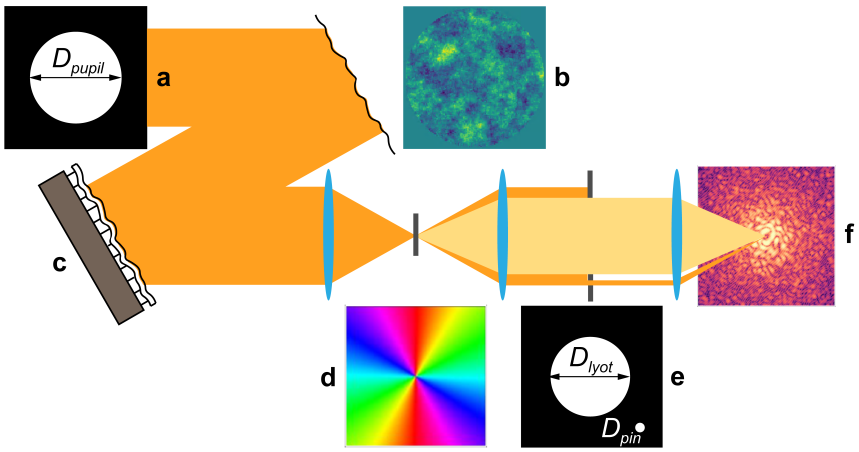

Figure 2. Basic telescope and coronagraph instrument layout. The wavefront is first incident on (a) the telescope aperture wavefront with diameter D_{pupil} and is aberrated by (b) phase errors. The aberrated wavefront is then corrected by a (c) DM and sent to a (d) focal plane mask. A charge-6 vector vortex phase plate is used in this example. This diffracts on-axis starlight to the outer edge of the pupil, which is blocked by a (e) Lyot stop with a central aperture and reference pinhole diameters D_{lyot} and D_{pin}. Light from the reference channel causes speckles in the (f) final science image to be fringed.

2.2 Self-Coherent Camera Low-Order Response

First, we simulate the Zernike response of the SCC for a Lyot stop with dimensions of $D_{lyot} = 0.95D$ and $D_{pin} = 0.01D$. This was done by injecting Zernike's one at a time using the phase screen, simulating a science image, then measuring the Zernike response estimated by the SCC. The Lyot stop had the separation between the central aperture and pinhole set at $l = 1.55D$. The SCC response using this Lyot stop for Zernikes 2 through 25 is shown in Figure 3.

We can see that the SCC has a fairly linear response up to 0.025 waves of wavefront error, and tapers off by 0.05 waves of wavefront error. However, it is not responsive whatsoever to Zernikes 2 through 9, in addition to Zernike 11. This demonstrates why it is necessary to pair a complimentary LOWFS with the SCC, as it is not sensitive to these low-order errors.

2.3 Self-Coherent Camera Dimensions

In this section, we provide a brief discussion on SCC Lyot stop construction. Specifically, we examine how changing D_{lyot} and D_{pin} can impact dark hole contrast limits in the presence of static wavefront error injected

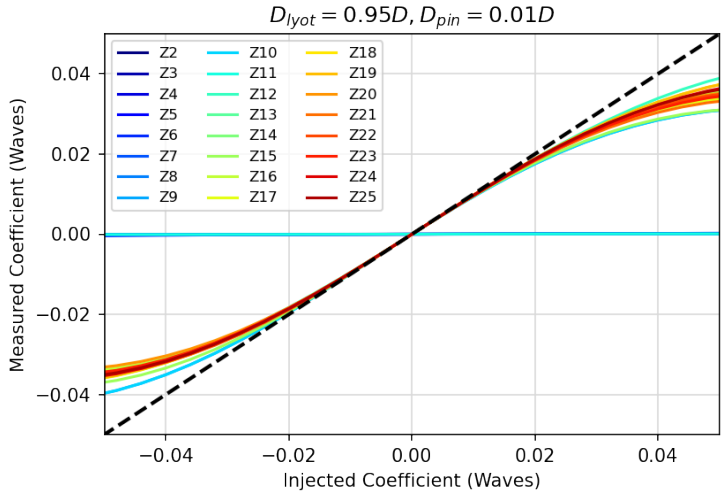

Figure 3. SCC Zernike response for $D_{lyot} = 0.95D$ and $D_{pin} = 0.01D$. The SCC is not responsive to Zernikes 2 through 9, and Zernike 11

using the phase screen. Whenever wavefront error was injected using the phase screen, Zernikes 2 through 9, and 11 were removed to emulate LOWFS and control. In this and all following experiments, contrast is defined as as average contrast within the dark hole. For each case, a half dark hole was dug between 2 and 10 λ/D, examples for which are seen in Figure 6.

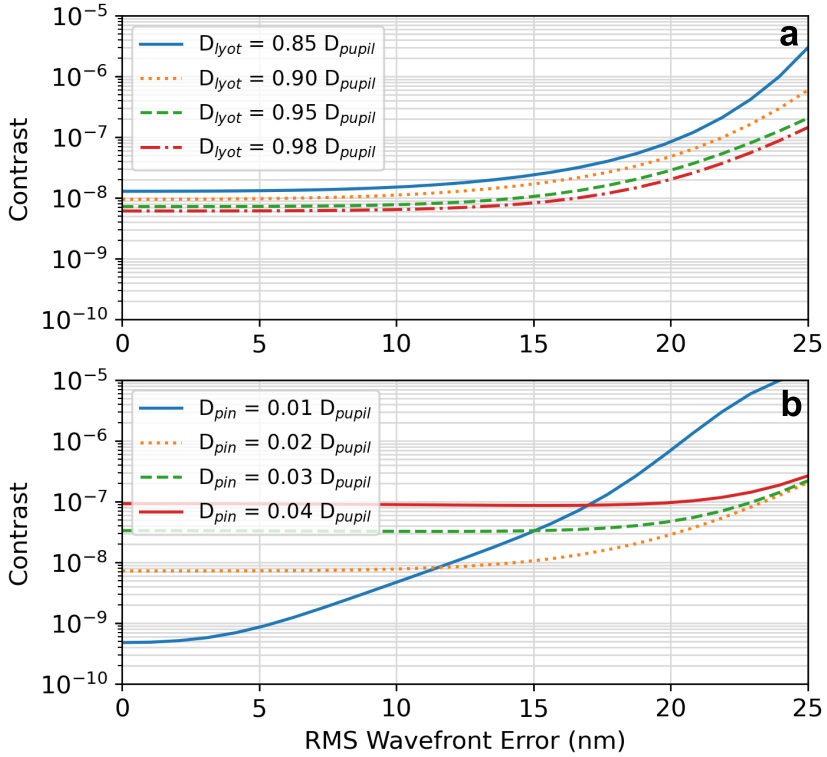

Figure 4. The SCC's tolerance to static errors is presented using contrast limits for different amounts of wavefront error while varying (a) D_{lyot} and (b) D_{pin}.

For the first experiment, D_{pin} was held constant at $0.02D_{pupil}$ whie D_{lyot} was varied. For each modified

Lyot stop, the SCC was first calibrated, then run for 30 iterations on an aberrated wavefront to dig a dark hole. The mean dark hole contrast after 30 iterations was recorded and plotted against injected wavefront error in Figure 4a below. The following experiment held D_{lyot} constant at $0.95D_{pupil}$ whie D_{pin} was varied. Again for each modified Lyot stop, the SCC was first calibrated, then run for 30 iterations on an aberrated wavefront to dig a dark hole. The mean dark hole contrast after 30 iterations was recorded and plotted against injected wavefront error in Figure 4b below. These experiments were simulated in the absence of photon or read noise.

Simulation results show that D_{lyot} has a noticeable impact on achievable contrast. As D_{lyot} increases, the contrast floor goes deeper and is maintained at larger injected wavefront errors as well. However, past $D_{lyot} = 0.98D_{pupil}$, contrast begins decreasing due to the Lyot stop no longer properly rejecting starlight.

D_{pin} has a much more pronounced effect on the contrast floor. In general, a smaller D_{pin} is desirable, as this limits the amount of excess light in the reference channel. However this comes at the price of sensitivity, as we can see contrast degrade significantly faster after 5 nm RMS of injected wavefront error for $D_{pin} = 0.01D_{pupil}$. This is caused by decreased fringe visibility, as less light in the reference channel means it can be more easily be washed out by stellar leakage.

3. SELF-COHERENT CAMERA TOLERANCES

3.1 Photon and Detector Read Noise

In this section, we analyze the SCC's tolerance to photon and detector read noise. For a $D_{pupil} = 6$ meter monolithic circular aperture, the total system throughput was assumed to be 25%. The detector was modeled after the Sony IMX571, with 1.23×10^{-4} e^-/second/pixel dark current and 1 e^- read noise at a sensor temperature of 20°C. We chose this over a traditional EMCCD detector as our lab has been exploring using CMOS detectors for a small, affordable cubesat coronagraph mission.[24] It is also the same detector model being used on our lab's new vacuum compatible vector vortex coronagraph testbed.[25,26]

5 nanometers RMS wavefront error was injected for each case using the phase screen. Using these parameters, the SCC was run for 200 iterations on a 5th magnitude star at various exposure times in order to demonstrate the impact of photon and detector read noise on achievable contrast.

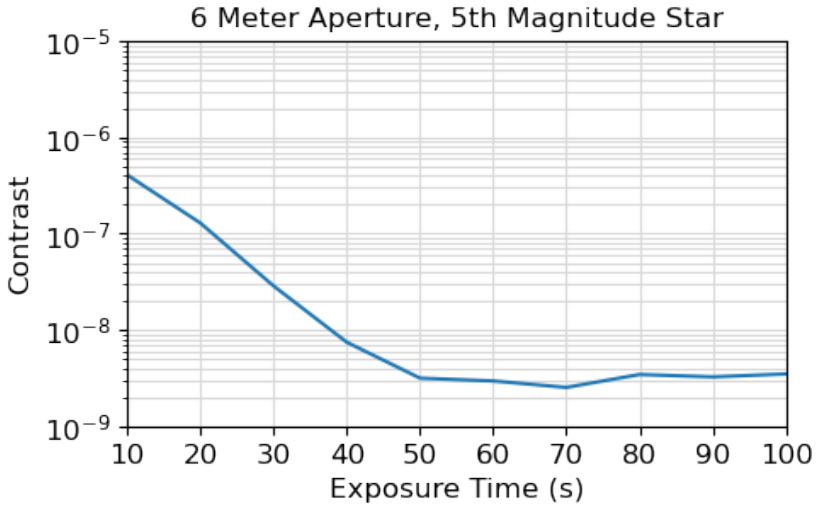

Figure 5. The SCC's tolerance to photon and detector read noise is presented for a 6 meter monolithic circular aperture with 5 nm RMS injected wavefront error. Dark hole contrasts after 200 SCC iterations on a 5th magnitude star are presented while varying exposure time.

We can see that an exposure time around 60 seconds is required to overcome photon and detector read noise on a 5th magnitude star. This result also highlights why observatory stability is key for high contrast imaging, as the wavefront needs to be stable during this exposure time so that the DM can remain correcting the wavefront between correction loop updates.

3.2 Observatory Pointing Errors

Last, we analyze the SCC's tolerance to observatory pointing errors in the presence of photon and detector read noise. These pointing errors manifest as beamwalk on intermediate optics not in a pupil plane. As the beam walks across these optics, it samples different regions of surface error which the DM is not calibrated to correct for, leading to degraded performance. For the same $D_{pupil} = 6$ meter monolithic circular aperture, the total system throughput was assumed to be 25% and a 60 second exposure time was used. The detector was again modeled using 1.23×10^{-4} e^-/second/pixel dark current and 1 e^- read noise. 5 nanometers RMS wavefront error was injected using the phase screen.

Beamwalk was modeled by translating the phase screen in simulation. 60 pointing offsets were drawn for a Gaussian distribution corresponding to 10 , 50, 100, and 500 milli-arcseconds per second RMS pointing error. These were converted to beamwalk values by assuming 1 millimeter of lateral translation per arcsecond of pointing offset. The total power at the image plane was summed for each offset and the detector was read out to create a science image which the SCC could then use to estimate the wavefront. Using this method, the SCC was run for a 30 minute acquisition on a 5th magnitude star to demonstrate continuous dark hole maintenance.

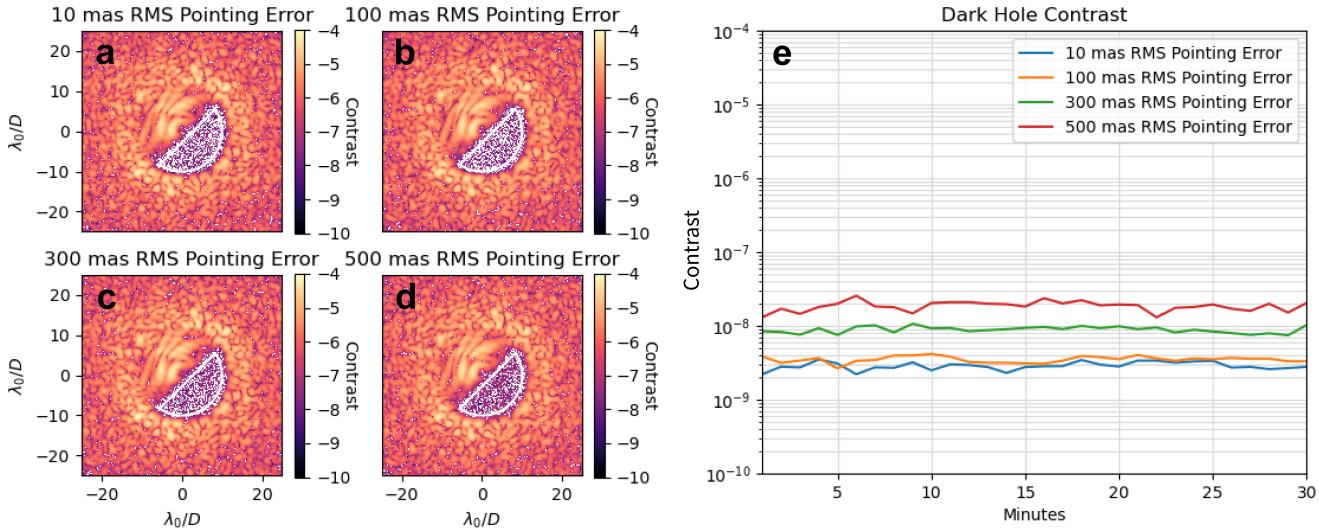

Figure 6. Representative images of dark holes being maintained in the presence of (a) 10, (b) 100, (c) 300, and (d) 500 milli-arcseconds RMS pointing error. (e) A plot of dark hole contrast over a simulated 30 minute acquisition for these pointing errors is also shown.

Figure 6 shows that the SCC can maintain dark hole contrast for extended acquisition times. We can see that pointing error greater than 100 milli-arcsec RMS lowers the contrast floor. This is because on a 5th magnitude star, 60 second exposure times are required overcome the photon noise limit. For large pointing errors over a long period, the beam is able to sample enough of the optical surface which is not being corrected by the DM to noticeably degrade performance.

4. CONCLUSION

We modeled a 6 meter unobstructed telescope and vector vortex coronagraph instrument at 550 nm with 2% bandwidth in HCIPy. We simulated the SCC response to the first 25 Zernike modes. The SCC was not sensitive to Zernikes 2 through 9, and 11, demonstrating the need for a complimentary low-order wavefront sensor (LOWFS) to be used with the SCC.

By simulating contrast limits for several modified Lyot stops in the presence of optical surface errors, we showed that the central aperture should be maximized and the pinhole diameter should be minimized for SCC performance. However, performance drops off considerably faster for smaller pinhole sizes after more than 5 nm RMS wavefront error is introduced.

Next, contrast limits on a 5th magnitude star using different detector exposure times were simulated. We show that 60 seconds exposure time using a CMOS detector is required to overcome photon noise limits. Finally, with the exposure time set at 60 seconds, we show how the maintainable contrast floor can be degraded by beamwalk. We demonstrate that for a 6 meter aperture and a 5th magnitude star, up to 50 milli-arcseconds per second RMS pointing error is tolerable.

The SCC provides an easy to implement and attractive solution for maintaining dark holes within coronagraphs. Future work will refine the optical model by considering multiple optical surfaces and taking Fresnel diffraction into account. Additionally, we will explore using the SCC on a segmented aperture using coronagraph instruments suggested for a future UVOIR flagship,[22] further advancing a key technology in the search for life beyond our solar system.

ACKNOWLEDGMENTS

Support for this work was provided by NASA through the NASA Hubble Fellowship grant #HST-HF2-51436.001-A awarded by the Space Telescope Science Institute, which is operated by the Association of Universities for Research in Astronomy, Incorporated, under NASA contract NAS5-26555. The authors would like to acknowledge the help of other members within both the Large Optics Fabrication and Testing Group and University of Arizona Space and Astrophysics Lab.

REFERENCES

[1] Guyon, O., "Extreme Adaptive Optics," *Annual Review of Astronomy and Astrophysics* **56**, 315–355 (Sept. 2018). Publisher: Annual Reviews.

[2] Oppenheimer, B. R. and Hinkley, S., "High-Contrast Observations in Optical and Infrared Astronomy," *Annual Review of Astronomy and Astrophysics* **47**, 253–289 (Sept. 2009).

[3] Krist, J. E., Gutt, G., Marchen, L., McGuire, J., Amiri, N., Nemati, B., Saini, N., Tang, H., Riggs, A., Marx, D., Sidick, E., and Zhou, H., "WFIRST coronagraph optical modeling," in [*Techniques and Instrumentation for Detection of Exoplanets VIII*], Shaklan, S., ed., 4, SPIE, San Diego, United States (Sept. 2017).

[4] Trauger, J. T., Moody, D. C., Krist, J. E., and Gordon, B. L., "Hybrid Lyot coronagraph for WFIRST-AFTA: coronagraph design and performance metrics," *Journal of Astronomical Telescopes, Instruments, and Systems* **2**, 011013 (Jan. 2016). Publisher: SPIE.

[5] Douglas, E. S., Males, J. R., Clark, J., Guyon, O., Lumbres, J., Marlow, W., and Cahoy, K. L., "Laser Guide Star for Large Segmented-aperture Space Telescopes. I. Implications for Terrestrial Exoplanet Detection and Observatory Stability," *The Astronomical Journal* **157**, 36 (Jan. 2019). Publisher: American Astronomical Society.

[6] Stover, J. C., [*Optical scattering. Measurement and analysis*] (Jan. 1995). Publication Title: SPIE Press Volume ADS Bibcode: 1995osma.book.....S.

[7] Breckinridge, J. B., Lam, W. S. T., and Chipman, R. A., "Polarization Aberrations in Astronomical Telescopes: The Point Spread Function," *Publications of the Astronomical Society of the Pacific* **127**, 445–468 (May 2015).

[8] Males, J. R., Close, L. M., Miller, K., Schatz, L., Doelman, D., Lumbres, J., Snik, F., Rodack, A., Knight, J., Van Gorkom, K., Long, J. D., Hedglen, A., Kautz, M., Jovanovic, N., Morzinski, K., Guyon, O., Douglas, E., Follette, K. B., Lozi, J., Bohlman, C., Durney, O., Gasho, V., Hinz, P., Ireland, M., Jean, M., Keller, C., Kenworthy, M., Mazin, B., Noenickx, J., Alfred, D., Perez, K., Sanchez, A., Sauve, C., Weinberger, A., and Conrad, A., "MagAO-X: project status and first laboratory results," (July 2018). arXiv:1807.04315 [astro-ph].

[9] Mendillo, C. B., Howe, G. A., Hewawasam, K., Martel, J., Finn, S. C., Cook, T. A., and Chakrabarti, S., "Optical tolerances for the PICTURE-C mission: error budget for electric field conjugation, beam walk, surface scatter, and polarization aberration," in [*Techniques and Instrumentation for Detection of Exoplanets VIII*], Shaklan, S., ed., 34, SPIE, San Diego, United States (Sept. 2017).

[10] Blaurock, C., McGinnis, M., Kim, K., and Mosier, G. E., "Structural-thermal-optical performance (STOP) sensitivity analysis for the James Webb Space Telescope," 58670V (Aug. 2005).

[11] Groff, T. D., Eldorado Riggs, A. J., Kern, B., and Jeremy Kasdin, N., "Methods and limitations of focal plane sensing, estimation, and control in high-contrast imaging," *Journal of Astronomical Telescopes, Instruments, and Systems* **2**, 011009 (Dec. 2015).

[12] Pueyo, L., Kay, J., Kasdin, N. J., Groff, T., McElwain, M., Give'on, A., and Belikov, R., "Optimal dark hole generation via two deformable mirrors with stroke minimization," *Applied Optics* **48**, 6296 (Nov. 2009).

[13] Give'on, A., Kern, B., Shaklan, S., Moody, D. C., and Pueyo, L., "Broadband wavefront correction algorithm for high-contrast imaging systems," 66910A (Sept. 2007).

[14] Potier, A., Baudoz, P., Galicher, R., Singh, G., and Boccaletti, A., "Comparing focal plane wavefront control techniques:\\Numerical simulations and laboratory experiments," *Astronomy & Astrophysics* **635**, A192 (Mar. 2020). arXiv: 2003.04336.

[15] Mazoyer, J., Baudoz, P., Galicher, R., and Rousset, G., "High-contrast imaging in polychromatic light with the self-coherent camera," *Astronomy & Astrophysics* **564**, L1 (Apr. 2014). arXiv: 1402.5914.

[16] Galicher, R., Baudoz, P., Rousset, G., Totems, J., and Mas, M., "Self-coherent camera as a focal plane wavefront sensor: simulations," *Astronomy and Astrophysics* **509**, A31 (Jan. 2010).

[17] Galicher, R., Baudoz, P., and Rousset, G., "Wavefront error correction and Earth-like planet detection by a self-coherent camera in space," *Astronomy & Astrophysics* **488**, L9–L12 (Sept. 2008).

[18] Baudoz, P., Boccaletti, A., Baudrand, J., and Rouan, D., "The Self-Coherent Camera: a new tool for planet detection," *Proceedings of the International Astronomical Union* **1**, 553–558 (Oct. 2005).

[19] Bottom, M., Wallace, J. K., Bartos, R. D., Shelton, J. C., and Serabyn, E., "Speckle suppression and companion detection using coherent differential imaging," *Monthly Notices of the Royal Astronomical Society* **464**, 2937–2951 (Jan. 2017).

[20] Gerard, B. L., Marois, C., and Galicher, R., "Fast Coherent Differential Imaging on Ground-based Telescopes Using the Self-coherent Camera," *The Astronomical Journal* **156**, 106 (Aug. 2018).

[21] Jovanovic, N., Absil, O., Baudoz, P., Beaulieu, M., Bottom, M., Cady, E., Carlomagno, B., Carlotti, A., Doelman, D., Fogarty, K., Galicher, R., Guyon, O., Haffert, S., Huby, E., Jewell, J., Keller, C., Kenworthy, M. A., Knight, J., Kuhn, J., Miller, K., Mazoyer, J., N'Diaye, M., Por, E., Pueyo, L., Riggs, A. J. E., Ruane, G., Sirbu, D., Snik, F., Wallace, J. K., Wilby, M., and Ygouf, M., "Review of high-contrast imaging systems for current and future ground-based and space-based telescopes II. Common path wavefront sensing/control and Coherent Differential Imaging," 18.

[22] Decadal Survey on Astronomy and Astrophysics 2020 (Astro2020), Space Studies Board, Board on Physics and Astronomy, Division on Engineering and Physical Sciences, and National Academies of Sciences, Engineering, and Medicine, [*Pathways to Discovery in Astronomy and Astrophysics for the 2020s*], National Academies Press, Washington, D.C. (2021). Pages: 26141.

[23] Por, E. H., Haffert, S. Y., Radhakrishnan, V. M., Doelman, D. S., van Kooten, M., and Bos, S., "High Contrast Imaging for Python (HCIPy): an open-source adaptive optics and coronagraph simulator," in [*Adaptive Optics Systems VI*], Schmidt, D., Schreiber, L., and Close, L. M., eds., 152, SPIE, Austin, United States (July 2018).

[24] Maier, E. R., Douglas, E. S., Kim, D. W., Su, K., Ashcraft, J. N., Breckinridge, J. B., Choi, H., Choquet, E., Connors, T. E., Durney, O., Gonzales, K. L., Guthery, C. E., Haughwout, C. A., Heath, J. C., Hyatt, J., Lumbres, J., Males, J. R., Matthews, E. C., Milani, K., Montoya, O. M., N'Diaye, M., Noenickx, J., Pogorelyuk, L., Ruane, G. J., Schneider, G., Smith, G. A., and Stark, C. C., "Design of the vacuum high contrast imaging testbed for CDEEP, the Coronagraphic Debris and Exoplanet Exploring Pioneer," in [*Space Telescopes and Instrumentation 2020: Optical, Infrared, and Millimeter Wave*], Lystrup, M., Batalha, N., Tong, E. C., Siegler, N., and Perrin, M. D., eds., 198, SPIE, Online Only, United States (Dec. 2020).

[25] Ashcraft, J. N., Douglas, E. S., Derby, K. Z., Choi, H., Van Gorkom, K., Anche, R., Durney, O., Haffert, S., Harrison, L., Kautz, M., Kim, D., Lumbres, J., Males, J. R., Milani, K., Montoya, O. M., and Smith, G. A., "The space coronagraph optical bench (scoob): 1. design and assembly of a vacuum-compatible coronagraph testbed for spaceborne high-contrast imaging technology," in [*Space Telescopes and Instrumentation 2022: Optical, Infrared, and Millimeter Wave*], SPIE, Online Only, United States (2022).

[26] Van Gorkom, K., Douglas, E. S., Ashcraft, J. N., Haffert, S., Kim, D., Choi, H., Anche, R., Males, J. R., Milani, K., Derby, K. Z., Harrison, L., and Durney, O., "The space coronagraph optical bench (scoob): 2. wavefront sensing and control in a vacuum-compatible coronagraph testbed for spaceborne high-contrast imaging technology," in [*Space Telescopes and Instrumentation 2022: Optical, Infrared, and Millimeter Wave*], SPIE, Online Only, United States (2022).